The Affects of Halide Modifiers on the Sorption Kinetics of the Li-Mg-N-H System

Christine J. Erdy-Price, Joshua R. Gray, Robert J. Lascola and Donald L Anton*
Savannah River National Laboratory, Aiken, SC, USA

Savannah River National Laboratory
Aiken, SC 29803

* Author to whom correspondence should be addressed; Tel.: +1-803-507-8551; Fax: +1-803-652-8137

E-mail address:Donald.Anton@srnl.doe.gov

Abstract

In this present work, the affects of different transition metal halides ($TiCl_3$, VCl_3, $ScCl_3$ and $NiCl_2$) on the sorption properties of the 1:1 molar ratio of $LiNH_2$ to MgH_2 are investigated. The modified mixtures were found to contain $LiNH_2$, MgH_2 and LiCl. TGA results showed that the hydrogen desorption temperature was reduced with the modifier addition in this order: $TiCl_3$>$ScCl_3$>VCl_3>$NiCl_2$. Ammonia release was not significantly reduced resulting in a weight loss greater than the theoretical hydrogen storage capacity of the material. The isothermal sorption kinetics of the modified systems showed little improvement after the first dehydrogenation cycle over the unmodified system but showed drastic improvement in rehydrogenation cycles. XRD and Raman spectroscopy identified the cycled material to be composed of LiH, MgH_2, $Mg(NH_2)_2$ and Mg_3N_2.

Key words: Hydrogen storage; Amides; Metal Hydrides; Kinetics; Raman; XRD

1 Introduction

In a study of more than 300 destabilization reactions using first principle density function theory (DFT), Alapati *et al.* predicted that the reaction between 1:1 MgH_2 and $LiNH_2$ was energetically favorable with an enthalpy of 31.9 kJ/molH_2 [1]. In 2007, Lu *et al.* showed that the reaction between MgH_2 and $LiNH_2$ in a 1:1 molar ratio a new nitride-binary light metal nitride, LiMgN, was created for hydrogen storage applications [2]. The initial dehydrogenation reaction pathway was identified as:

$$LiNH_2 + MgH_2 \rightarrow LiMgN + 2H_2 \quad (1)$$

This 1:1 molar ratio of MgH_2 to $LiNH_2$ mixture has a theoretical hydrogen storage capacity of 8.2 wt%. The experimental heat of reaction was measured to be 33.5 kJ/mol H_2 [2], very close to the predicted enthalpy.

Through first-principle calculations of total energies and vibrations free energies, it was suggested that the initial decomposition of 1:1 $LiNH_2$: MgH_2 will proceed as in the following reaction steps [3]:

$$LiNH_2 + MgH_2 \rightarrow LiH + \tfrac{1}{2} Mg(NH_2)_2 + \tfrac{1}{2} MgH_2 \quad (2)$$

$$\rightarrow LiH + \tfrac{1}{4} Mg(NH_2)_2 + \tfrac{1}{4} Mg_3N_2 + H_2 \quad (3)$$

$$\rightarrow \tfrac{1}{2} LiH + \tfrac{1}{4} Mg_3N_2 + \tfrac{1}{4} Li_2Mg(NH)_2 + \tfrac{3}{2} H_2 \quad (4)$$

$$\rightarrow LiMgN + 2H_2 \quad (5)$$

The first predicted decomposition step would be the exothermic formation of magnesium amide. In the next step, half of the MgH_2 and half of the $Mg(NH_2)_2$ would form Mg_3N_2 through the endothermic reaction, releasing H_2 with an enthalpy of 15 kJ/mol H_2 [3]. The third step is a decomposition reaction which produces a mixed Li-Mg imide with an enthalpy of 47 kJ/mol H_2 [3]. Finally, the ternary nitride is formed with an enthalpy of 80 kJ/mol H_2 at 227°C. However, the proposed rehydrogenation and subsequent dehydrogenation process of LiMgN produces LiH, $Mg(NH_2)_2$ and MgH_2, as [2]:

$$LiMgN + 2H_2 \leftrightarrow \tfrac{1}{2} Mg(NH_2)_2 + \tfrac{1}{2} MgH_2 + LiH \quad (6)$$

Transition metals have been shown to significantly improve kinetics and reduction of dehydrogenation temperatures in many hydrogen storage systems, including $NaAlH_4$ [4-6], MgH_2 [7-10], the 1:1 MgH_2:$LiNH_2$ [2, 11] and 2:1 $LiNH_2$:MgH_2 [12]. Through the electronic structure and total energy calculation using first principle calculations on the effect of titanium on MgH_2, Song et al. found that the bond between magnesium and hydrogen was weakened [13]. Liang et al. investigated the impact of transition metals on hydrogen desorption of MgH_2 at 300°C and found that the transition metal chemisorbs hydrogen and transfers it to the Mg matrix creating a nucleation site for the hydride phase [10]. Lu et al. observed an increase in hydrogen absorption kinetics of 1:1 $LiNH_2$:MgH_2 with the addition of 4 wt% $TiCl_3$ resulting in an increase in capacity from 5 wt% to 7.9 wt% [2]. For the 2:1 $LiNH_2$:MgH_2 system, through density of states analysis, Wang et al. found that the N-H bonds were weakened by a Ti atom substituted by a Li atom and the decreased energy value of Li vacancy formation indicated improvement in rehydrogenation of $Li_2MgN_2H_2$ with Ti additive [12].

One issue related to the application of metal-N-H storage systems is ammonia formation that takes place simultaneously with H_2 release [14, 15]. Through the use of Draeger tubes on the 2:1 $LiNH_2$:MgH_2 system, Luo et al. showed that ammonia concentration was strongly dependent on the desorption temperature with concentrations

of 180ppm measured at 180°C and 720ppm at 240°C [15]. In a separate analysis, the effect of milling duration on ammonia release from the 2:1 mixture during heating was investigated, resulting in over 30 ppm/mg for unmilled samples and under 10 ppm/mg for samples milled for 180 minutes using high-energy milling [16].

In this present article, we report the effects of different metal halide additions on the ammonia release and isothermal sorption kinetics of the 1:1 $LiNH_2$:MgH_2 system. The influence of these halides has been investigated using thermogravimetric analysis (TGA), isothermal kinetics, x-ray diffraction (XRD) and Raman spectroscopy.

2 Experimental details

The starting materials, lithium amide ($LiNH_2$, 95 % purity, Aldrich), magnesium hydride (MgH_2, >97% purity, Gelest Inc), titanium chloride ($TiCl_3$, 99%, Aldrich), nickel chloride ($NiCl_2$, 99%, Aldrich), scandium chloride ($ScCl_3$, 99 %, Aldrich) and vanadium chloride (VCl_3, 99%, Aldrich) were purchased and used without alteration. Mixtures of $LiNH_2$ and MgH_2 with and without 1.5 mol% of the transition metal halides were prepared using Fritch planetary milling technique. Three grams of mixtures were loaded into the milling jars in the argon glove box while maintaining a 30:1 ball to sample weight ratio. The powders were milled for 2 hours with 30 minute cycles at 500 rpm.

Desorption properties were monitored as a function of temperature and time using a thermogravimetric analyzer (TGA) coupled with a residual gas analyzer (RGA). The TGA was located inside an argon glove box to prevent the samples from oxidizing. Eight milligram samples were loaded into a stainless steel microbalance pan and heated from 30°C to 400°C with a heating rate of 5°C /min under a constant flow of argon gas. The effluent gases from the TGA were constantly monitored for H_2, NH_3, H_2O and O_2 using a Hiden Analytical residual gas analyzer (RGA).

Hydrogen desorption and absorption kinetics measurements were carried out using a Sievert's apparatus (PCTPro-2000, Setaram). Approximate 0.5 gram samples were loaded into a stainless steel reactor vial and sealed in a glovebox. Standard isothermal discharge procedure called for heating of the sample under 110 bar or greater, in order to prevent premature hydrogen release to occur while heating. Once the desired discharge temperature was reached, the sample was discharged into the largest reservoir, 1170 mL, into a backpressure of 1 bar. During subsequent recharging cycles, the sample was heated to 180°C under active vacuum and then exposed to 100 bar of H_2 pressure. During the dehydrogenation and hydrogenation cycles, the sample temperature and reservoir pressure were recorded. The amount of H_2 discharge and uptake was determined from the changes in pressure within the calibrated volume reservoirs. A blank reactor vial was run under standard discharge conditions to identify the effects of gas thermal expansion during heating and volume expansion.

Powder x-ray diffraction (XRD) patterns of the as-milled, dehydrogenated and rehydrogenated materials were collected using a Rigaku Dmax/2100 (Cu K_α radiation). The samples were mounted on a glass slide and covered with Kapton® film while under

argon. The XRD patterns were recorded at 2θ spanning 5 to 80° with a scanning rate of 0.02°/min.

Raman spectra were obtained with 532 nm excitation (Verdi-2W, Coherent, Inc.) in the backscattering mode, using an imaging probe (MultiRxn Probe, Kaiser Optical Systems) with a 5 mm working distance. Excitation powers were restricted to less than 20 mW at the sample, in a spot approximately 200 μm in diameter, to avoid sample degradation. No sample changes were visible after irradiation under these conditions. Scattered light was detected with a holographic spectrometer (Holospec VPH, Kaiser Optical Systems) and CCD camera (DV420A, Andor) electrically cooled to -55 ^{o}C. Spectral resolution is 4-6 cm^{-1}, with a shift accuracy of ± 1 cm^{-1}. Spectra were measured at room temperature (approximately 20^{o}C). Samples were contained in a sealed quartz vial; contributions of the vial to the spectra were subtracted. These samples exhibited a large background signal, probably due to scattering by metallic Mg (present in the MgH_2 source) and/or Ti (from $TiCl_3$ in the modified samples). The background was simulated by fitting to a polynomial and then subtracted. Despite this step, some of the weaker Raman bands presumed to be present (e.g. for MgH_2) could not be recovered.

3 Results and Discussion

3.1 *Characterization of As-milled Systems*

Figure 1 compares the XRD patterns of the unmodified, $TiCl_3$ and $ScCl_3$ modified mixtures after milling. Identification of LiCl peaks clearly shows that the halide addition promoted initial decomposition of $LiNH_2$. This was a typical observation for all the 1:1 $LiNH_2$:MgH_2 mixtures with transition metal halide modifiers. Furthermore, the unmodified mixture showed no indication of such a decomposition, which is in agreement with the results from Liu *et al.*, who observed the absence of gas evolution for milling times under 12 hours at 500 rpm [17].

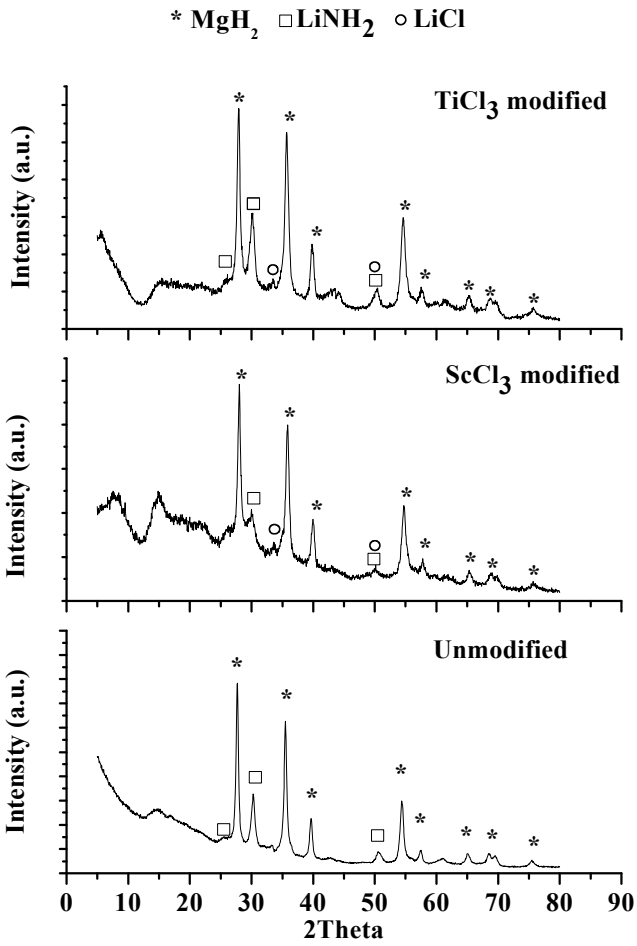

Figure 1. XRD analysis of unmodified (bottom), $ScCl_3$ (middle) and $TiCl_3$ (top) modified 1:1 $LiNH_2$:MgH_2 after 2 hours of Fritsch milling at 500rpm.

3.2 *Decomposition of the modified and unmodified systems*

The TGA curves of the unmodified and modified materials show that the weight loss of the modified mixture starts at lower temperatures than the unmodified, as seen in Figure 2. The slight increase in weight percent observed at the beginning of the TGA curves are attributed to a buoyancy effect as the carrier gas is heated.

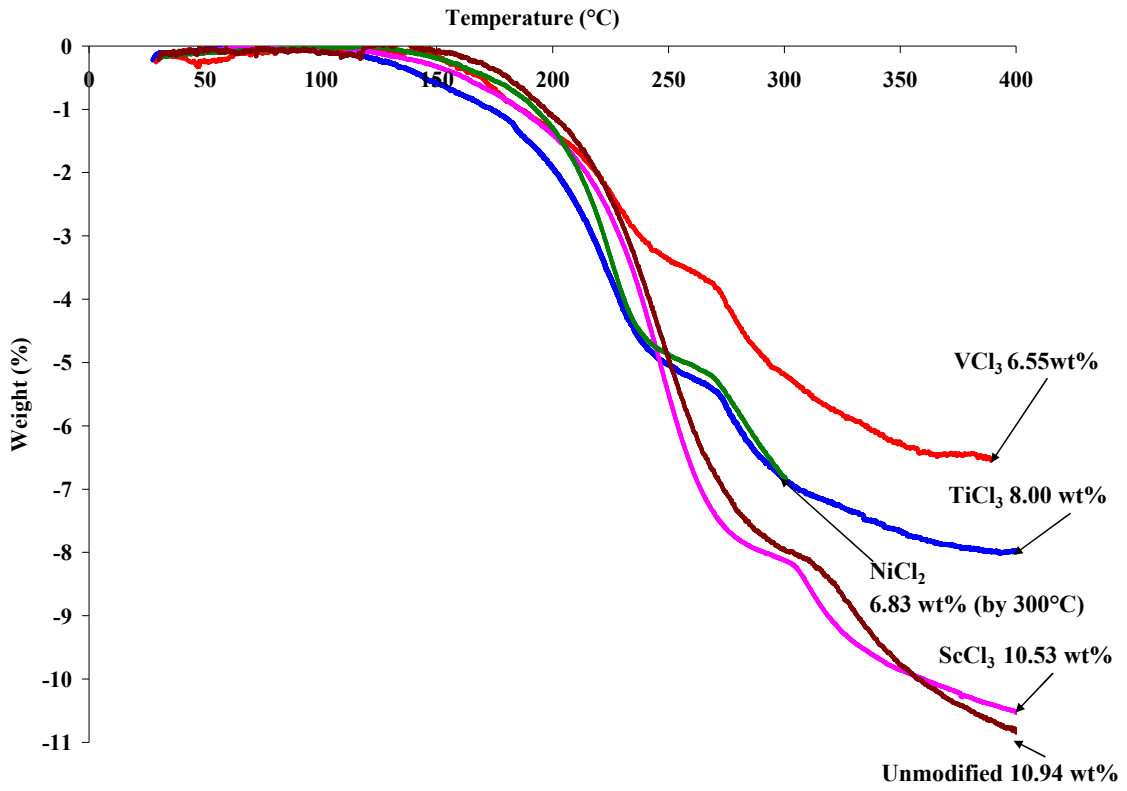

Figure 2. TGA analysis of the decomposition of unmodified and modified 1:1 $LiNH_2$:MgH_2 mixture at a heating rate of 5°C/min.

By determining the derivative of weight change with time over time, the initial hydrogen desorption temperature of the unmodified mixture was determined to be in the range of 135 to 145°C, which is slightly higher than the initial desorption temperature observed by Lu *et al*. of 120°C whom utilized the rolling jar mill for 24 hours technique for materials synthesis [2]. The ability of the metal halides to reduce the initial temperature of desorption follows the order: $TiCl_3$>$ScCl_3$>VCl_3>$NiCl_2$. The approximate ranges for the modified samples are listed in Table 1.

The RGA results of hydrogen gas composition during the TGA experiments are given in Figure 3. This data show the unmodified material decomposition is comprised of three hydrogen releases steps. Between 135 and 145°C, the initial hydrogen release peaked at approximately 205°C during which 1wt% of the sample was lost. The second hydrogen release peaked at 260°C. During this time, a total of 6.48 wt% was lost. It was during this step that NH_3 also peaked at 265°C, as illustrated in Figure 4. A similar ammonia emission temperature was observed by Liang, *et al.* for a 1:1 $LiNH_2$:MgH_2 milled for 2 hours [18]. The third hydrogen release peaked at 340°C. The unmodified mixture lost a total of 10.94 wt% during decomposition, which is significantly higher than the theoretical hydrogen capacity of 8.14 wt%. This increase is attributed to release of ammonia from the decomposition of unreacted $LiNH_2$ and the slow reaction kinetics between MgH_2 and NH_3 [15, 16].

The total weight lost by the 1:1 $LiNH_2$:MgH_2 mixture with 1.5 mol% $TiCl_3$ is 8.00 wt%, which is slightly higher than the theoretical hydrogen capacity of 7.85 wt%.

From Table 1, the range of initial hydrogen release is between 90 and 100°C, which is a significant reduction in temperature from the unmodified mixture. The other hydrogen releases were also shifted to lower temperatures indicating that the $TiCl_3$ promoted the dehydrogenation reaction, as depicted in Figure 3. Ammonia release peaked at approximately 245°C, as illustrated Figure 4, which is a 20°C reduction from the unmodified The sample containing VCl_3, where initial H_2 release occurred between 110 and 120°C, showed very similar reduction in peak hydrogen and ammonia release temperatures. However, as seen in Table 1, the measured weight loss was significantly lower than the theoretical capacity indicating possible hydrogen release during milling.

The addition of $ScCl_3$ significantly impacted the 1:1 $LiNH_2$:MgH_2 mixture, resulting in the largest weight loss of the modified samples with 10.53 wt%, which is nearly 40 % larger than its theoretical H_2 capacity of 7.48 %. It also resulted in only 2 peak hydrogen releases, as shown in Figure 3. The first hydrogen release peaked at 270°C with a total of 8.3 wt% lost, which included both H_2 and NH_3 emission. The peak ammonia release temperature was at approximately 280°C, which is a 15°C increase from the unmodified sample. The second peak hydrogen release was at approximately 335°C where the remaining weight loss was attributed to hydrogen release.

From the addition of transition metal halides, the initial hydrogen desorption temperature of the 1:1 $LiNH_2$:MgH_2 system was reduced. As seen in Table 1, the initial hydrogen desorption for the modified systems began between 90°C and 120°C, which is lower than the release temperature of 135°C for the unmodified material, with $TiCl_3$ and $ScCl_3$ having the largest effect on temperature reduction. From literature, scandium has been shown to dissociate the Mg-H bonds since Sc has the lowest 3d orbital occupancy among the 3d transition metals which largely contributes to the donation of the electrons from the bonding orbitals to MgH_2 [19] This suggests that Ti and Sc are more effective at allowing the conversion of $LiNH_2$ and MgH_2 to LiH, $Mg(NH_2)_2$ and H_2 to occur at a lower temperature by weakening the Mg-H bond. However, it is important to note that the $NiCl_2$ modified sample showed the largest hydrogen release prior to 300°C, which peaked at 275°C. This is also similar to the results reported by Tsuda et al., who showed that the high 3d orbital occupancy of Ni contributes to the back-donation of the electrons to the antibonding orbitals of MgH_2 allowing for easier Mg-H dissociation [19].

Additive compositions also greatly affected ammonia release. As seen in Figure 4, the mixtures with $TiCl_3$ and VCl_3 released ammonia at temperatures lower than the unmodified material, while the mixtures modified with $ScCl_3$ and $NiCl_2$ increased the temperature. As seen by the XRD pattern for the $TiCl_3$ and $ScCl_3$ samples, in Figure 1, LiCl formed during milling via a metathesis reaction between $LiNH_2$ and the halide. It is possible that during decomposition, the metathesis reaction was promoted, resulting in the further formation of LiCl and release of NH_3. Also, as stated by Liang *et al.*, ammonia release could be the result from thermal self-decomposition of $LiNH_2$ due to its large particle size and uneven mixing with MgH_2 cause by the short milling time [18].

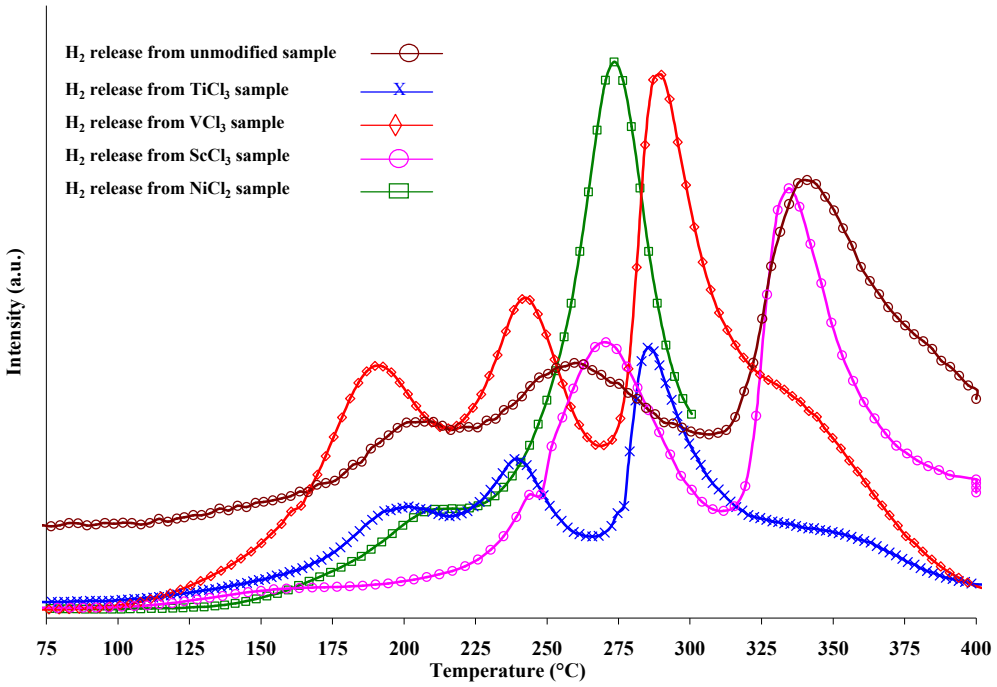

Figure 3. RGA curves of the hydrogen (Mass 2) release for the unmodified and modified 1:1 $LiNH_2$:MgH_2 mixtures after milling for 2 hours.

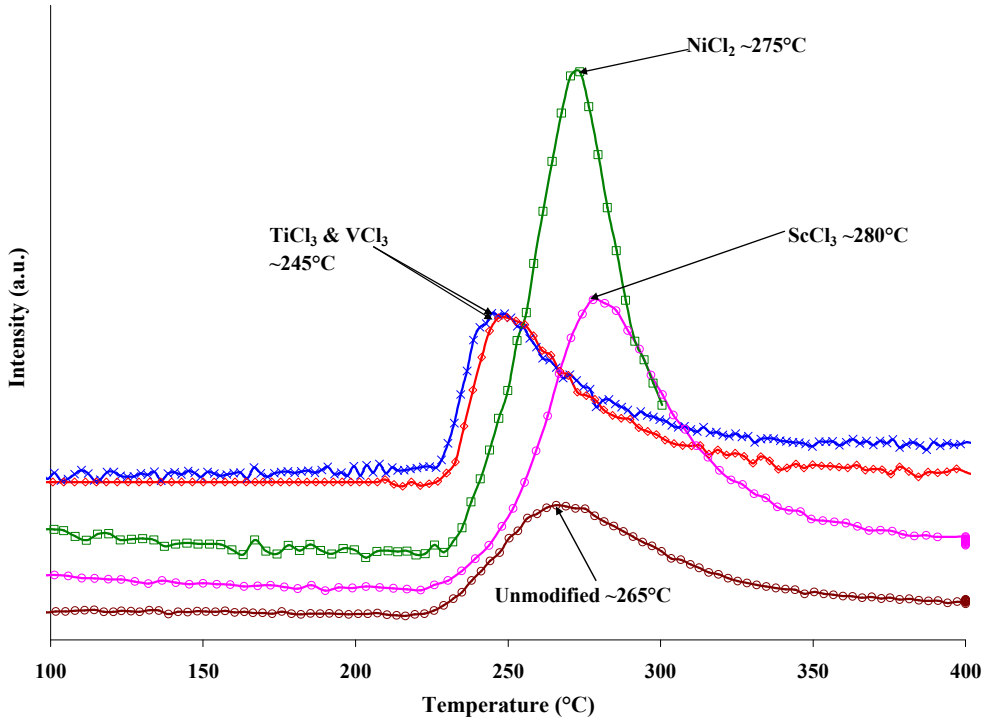

Figure 4. RGA curves of the ammonia release for the unmodified and modified 1:1 $LiNH_2$:MgH_2 mixtures after milling for 2 hours.

Table 1. Summary of TGA/RGA decomposition data of the as-milled 1:1 $LiNH_2$:MgH_2 samples with and without various modifiers while heating from RT to 400°C at 5°C/min.

Modification	Theoretical H_2 Wt %	Total Wt % Released	Approx. Initial H_2 Release (°C)	H^1 (°C)	H^2 (°C)	H^3 (°C)	Peak NH_3 Release Temperature (°C)
Unmodified	8.14	10.94	135 - 145	205	260	340	260
1.5 mol% $TiCl_3$	7.85	8.00	90-100	200	240	285	245
1.5 mol% VCl_3	7.46	6.55	110-120	190	240	290	245
1.5 mol% $ScCl_3$	7.48	10.53	110-115	-	270	335	280
1.5 mol% $NiCl_2$ (by 300°C)	7.57	6.83	120-130	210	275	-	270

3.2.1 Effect of Modifiers on Isothermal Sorption Kinetics

The impact of the modifiers on the kinetic performance during the isothermal sorption of 1:1 $LiNH_2$:MgH_2 was also investigated. The overall sorption rate during the first 30 minutes (0.5 hours) of the first and fourth dehydrogenation cycles are shown in Figure 5. The sharp change in slope observed during the first dehydrogenation cycle indicates a change in reaction mechanisms and kinetics.

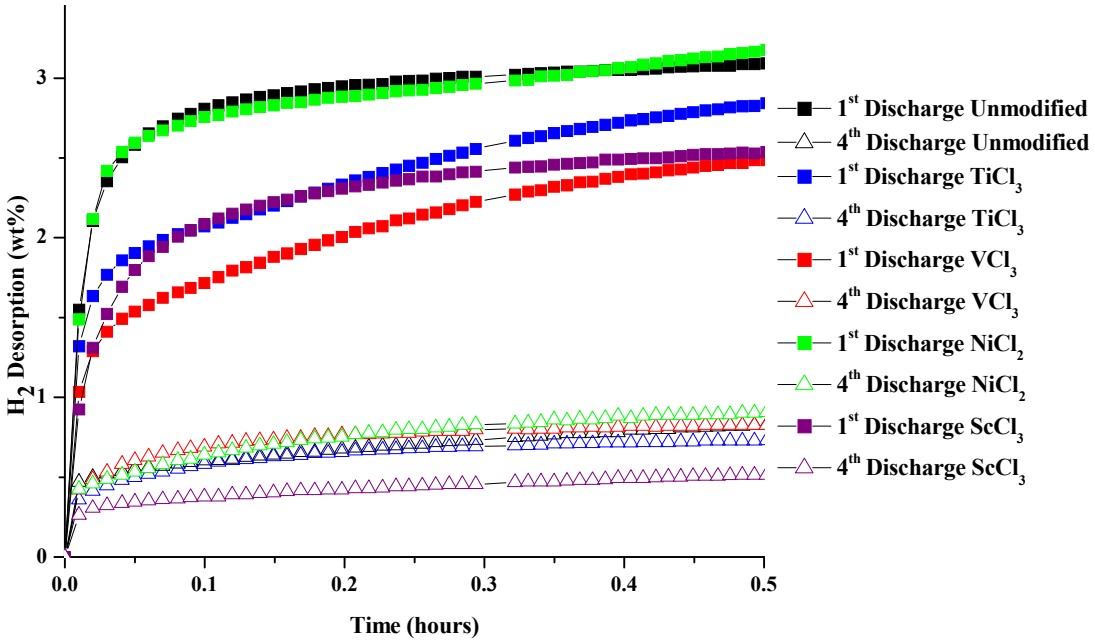

Figure 5. First (solid) and fourth (hollow) isothermal dehydrogenation curves at 260°C into 1 bar for the (black) unmodified and samples containing 1.5 mol% (blue) $TiCl_3$, (red) VCl_3, (green) $NiCl_2$ and (purple) $ScCl_3$ modifiers.

During the fourth dehydrogenation cycle, illustrated in Figure 5, a significant reduction in dehydrogenation kinetics is observed for all samples. The addition of the modifiers lowered the initial desorption temperature but they did not enhance the kinetics of the isothermal dehydrogenation reaction past the first desorption, which is similar to the results observed by Lohstroh *et al.* for $TiCl_3$ with the 2:1 $LiNH_2$:MgH_2 [20]. Over four cycles, the samples dehydrogenated 2.0 wt%, which is significantly lower than the theoretical hydrogen capacity for the system. Possible kinetic barriers to full capacity sorption are discussed below.

After each dehydrogenation cycles, vacuum was applied to the sample for 30 minutes while it cooled from 260°C to 180°C, providing a fully dehydrogenated sample. During the absorption cycles at 180°C, the samples recharged between 4 and 6 wt%, with the $ScCl_3$ and $NiCl_2$ modified sample having the highest absorption capacity followed by the unmodified, VCl_3 and $TiCl_3$ samples respectively.

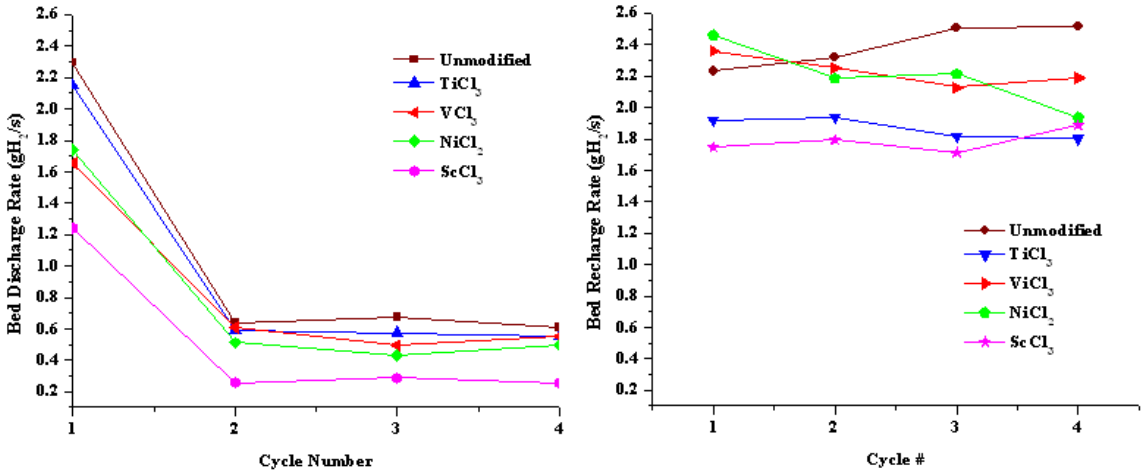

Figure 6. Overall bed discharge (A) and recharge (B) rates determined from isothermal dehydrogenation cycle at 260°C into 1 bar of back pressure and rehydrogenation cycle at 180°C under 100 bar hydrogen.

In order to compare the rates of charge and discharge to the DOE 2010 technical targets, the average sorption rate in grams of hydrogen per second per gram of media during the first 30 minutes of cycling was determined and reported here as $[gH_2/s]/kg_{material}$. This rate was then converted to bed discharge/charge rate using the estimated bed size, to hold 5 kg of H_2. The US DOE has set the goal of minimum charging rates of 20 g/sec. and discharging rates of 5 g/sec. for a 5 kg capacity storage system [21]. The current rates of sorption are significantly below these goals, as seen in Figure 6. One possible cause for low sorption rates is the possible loss of nitrogen through NH_3 emission and the formation of magnesium nitride, Mg_3N_2, which is the predominate product seen from XRD in Figure 7(A). Another cause could be the agglomeration of particle due to the high discharge temperature, as seen from the increase in average MgH_2 from 35.3 nm (as-milled) to 49.8 nm after cycling. Achievement of enhanced kinetics with minimal affect to capacity will be required to warrant further development and implementation of these materials.

3.2.2 Phase Identification

XRD analysis was performed after the second discharged at 260°C and the fourth rehydrogenation cycle at 180°C on the unmodified 1:1 $LiNH_2$:MgH_2. The XRD spectrum for the dehydrogenated sample shown Figure 7 in identifies cubic LiMgN and Mg_3N_2, similar to the results observed by Lu *et al.* [2, 11].

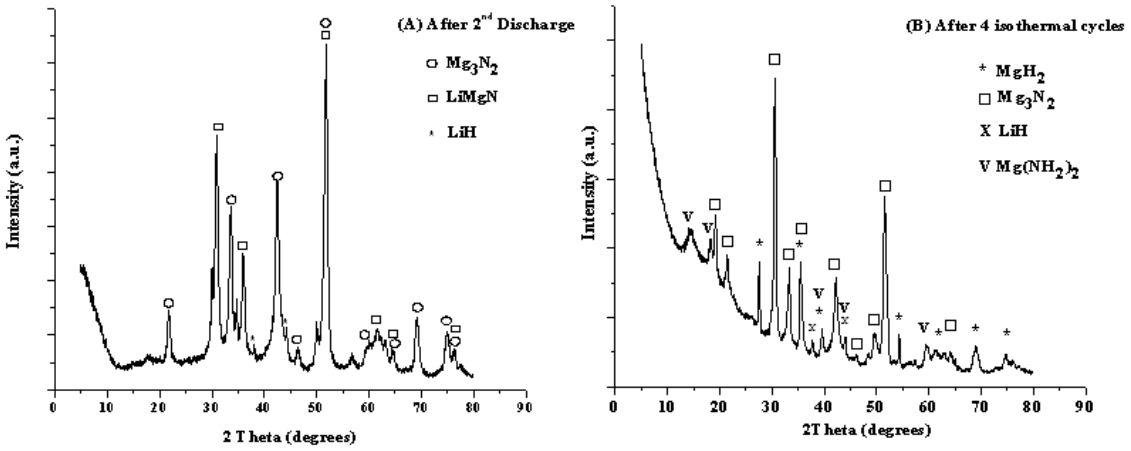

Figure 7. XRD pattern of 1:1 $LiNH_2$:MgH_2 without modifications (A) after 2nd desorption and (B) 4th absorption. The diffraction pattern of the dehydrogenated product is similar to that of cubic LiMgN identified by Lu *et al.*[2, 11] and Mg_3N_2 while the predominate components of the absorption pattern include MgH_2, LiH, $Mg(NH_2)_2$ and Mg_3N_2.

However, the $Li_2Mg_2(NH)_3$ observed by Osborn *et al.* after dehydrogenation at 210°C [22] was not observed. The XRD pattern of the hydrogenated sample after the 4th absorption cycle in Figure 7(B) shows that after the fourth rehydrogenation Mg_3N_2, MgH_2, LiH and $Mg(NH_2)_2$ are the dominant products. Here again, the $Li_2Mg_2(NH)_3$ phase seen by Lui *et al.* [17] in their rehydrogenated sample was not observed in the XRD pattern. The discrepancies with the reported literature were attributed different sample preparation techniques and cycling conditions.

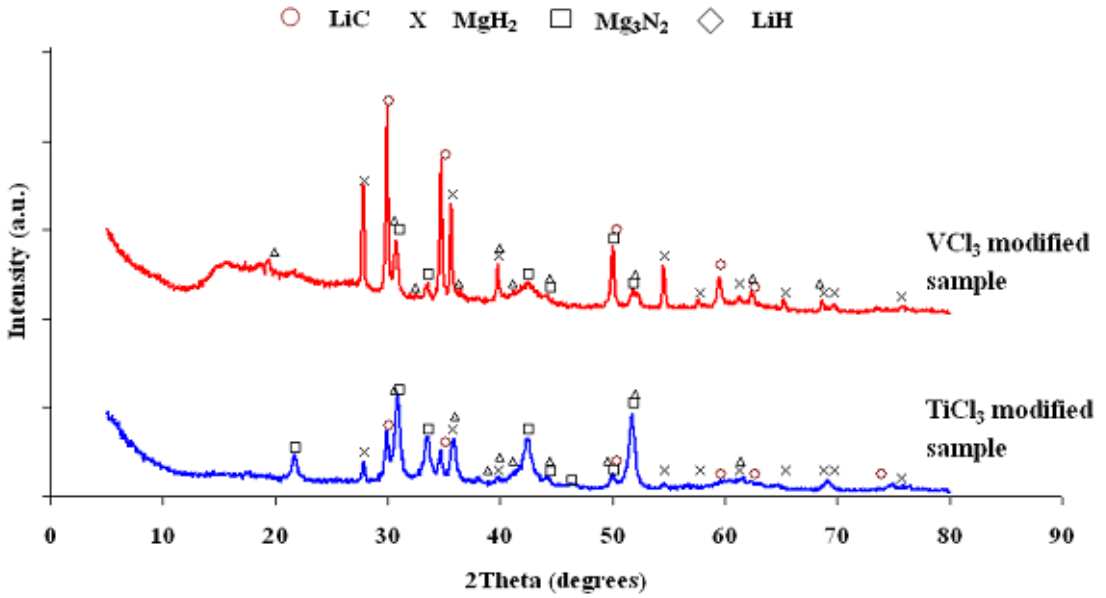

Figure 8. The XRD spectra after the 1st complete cycle of 1:1 $LiNH_2$:MgH_2 modified with 1.5 mol% $TiCl_3$ or VCl_3 showing the predominant recharged species to be MgH_2, LiH, and Mg_3N_2. Since the sample was not annealed before x-ray examination, $Mg(NH_2)_2$ peaks were not clearly identified. The peaks associated with LiCl are indicative of the metathesis reaction between $LiNH_2$ and the transition metal chlorides.

The XRD spectra after one complete isothermal cycle given in Figure 8 further illustrates the formation of salts, predominately LiCl as a result of cycling. The metathesis reaction results in the loss of essential nitrogen due to ammonia release, as possibly:

$$(x+1)LiNH_2 + TmCl_x \rightarrow xLiCl + Tm^{\circ} + xNH_3$$

thus preventing the reversible reaction from occurring. This metathesis reaction has been observed during the dry ball milling process of $NaAlH_4$ with $TiCl_3$, resulting in the reduction of $TiCl_3$ by the Na to form NaCl and metallic Ti [23]. Sandrock *et al.* went on to show that increasing the $TiCl_3$ loading resulted in an elimination of H-capacity with the formation of NaCl, Al and Ti, all of which do not store hydrogen [23].

To further identify the as-milled, dehydrogenated and hydrogenated phases, Raman spectroscopy was performed on the system modified with $TiCl_3$, with the results shown in Figure 9 (A) and (B). Raman spectra of the as-milled indicates the presence of unreacted $LiNH_2$ after milling. The vibrational bands observed at 3262 cm^{-1} (N-H symmetric stretch) and 3323 cm^{-1} (unresolved N-H asymmetric stretch doublet) match literature spectra of the pure material [9, 19]. Weak low-frequency (<500 cm^{-1}) bands associated with lattice translational and librational modes are not visible, most likely due to low measurement sensitivity against a large scattering background. A very weak peak observed at ~950 cm^{-1} is consistent with the expected MgH_2 vibration at 954 cm^{-1} [24], but is not definitive. However, no other peaks appear in this region of the spectrum that would suggest the presence of other reaction products.

The dehydrogenated sample was taken after the second discharge cycle and the rehydrogenated sample was taken after the fourth recharge cycle. As expected for the dehydrided sample, there is little or no Raman activity observable in the H-N-H stretching regions. The low-frequency region shows the growth of a clear doublet at 379

(strong) cm^{-1} and 341 (weak) cm^{-1}. These peaks are not coincident with the reported spectrum for LiMgN in which a single broad peak is observed at 492 cm^{-1}[25].

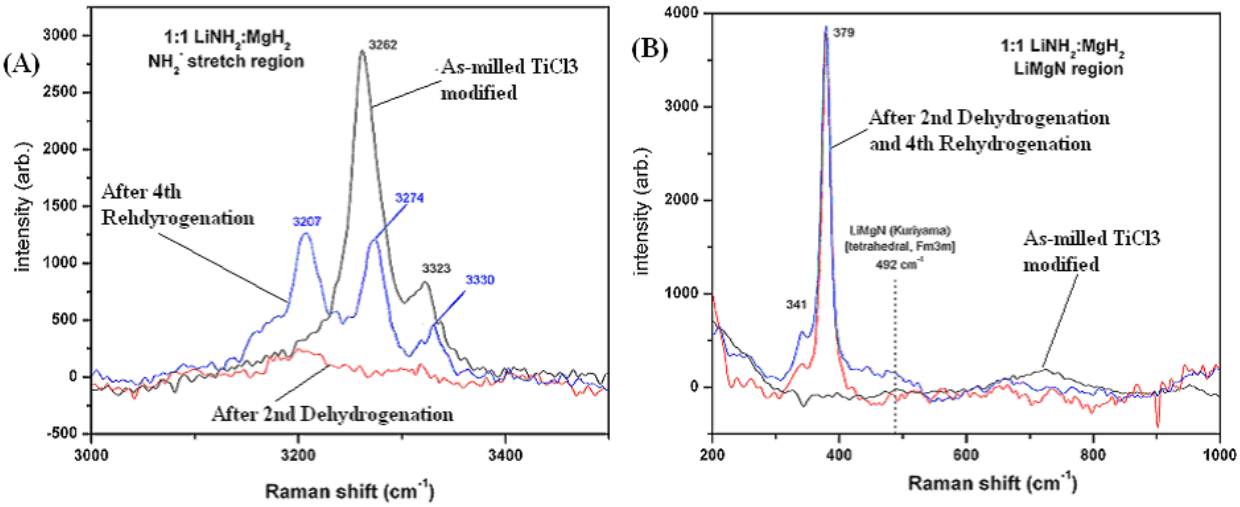

Figure 9. Raman spectra of the as-milled 1:1 $LiNH_2$:MgH_2 with $TiCl_3$ modifier in **(A)** the high-shift NH_2^- region and **(B)** the LiMgN region. The observed spectrum for the as-milled sample is consistent with high-shift stretches for $LiNH_2$. However, the observed LiMgN spectrum for the dehydrogenated sample was not consistent with literature [25]. The high-shift NH_2^- region for the rehydrogenated sample is consistent with the formation of $Mg(NH_2)_2$ and there is no evidence that $LiNH_2$ has been reformed indicating that the dehydrogenated sample did not rehydrogenate to the starting material

It is worth nothing that the spectrum observed doublet closely matches the strongest peaks in the reported spectrum of Mg_3N_2 [26]. The fate of the Li in the dehydrided sample is less clear. Yamane *et al.* noted that the insertion of Li into Mg_3N_2 to form $Li_{0.51}Mg_{2.49}N_{1.83}$ would reduce the space group from *Ia3* to *I213* [27]. The expected Raman spectrum of such a material could have more peaks, due to the reduction of symmetry, and the frequencies of the strongest peaks could be shifted due to the presence of Li. Neither effect is observed for this material. Additionally, the peaks are sharp, suggesting that there is little disorder in the material as might be expected for the random inclusion of Li. Overall, the Raman spectrum for the dehydrogenated sample does not permit a definitive identification of the dehydrided product or the creation of a new material; however, they are not good enough to rule it out.

The low-shift region of the Raman spectrum for the rehydrogenated sample (seen in Figure 9(A) is essentially identical to the dehydrided sample. The presence of the same doublet that is observed for the dehydrided material suggests that Mg_3N_2 and not LiMgN was formed during the dehydrogenation process. However, new peaks are observed in the N-H stretching region (Figure 9 (B)). The bands at 3274 $cm^{-1}$and 3330 cm^{-1} are consistent with the formation of $Mg(NH_2)_2$ [28] and echo the observation of that species in the XRD spectrum. There are no peaks that suggest the reformation of $LiNH_2$ (e.g. consistency with the spectrum of the as-mixed starting materials). As yet unidentified are the peak at 3207 cm^{-1} and the shoulder at ~3170 cm^{-1}. The other products identified in the XRD spectrum – MgH_2, LiH, and Mg_3N_2 – do not have Raman peaks in this region. Any candidate material(s) would have to be in an amorphous state or otherwise not be observable in the XRD spectrum. For example, the shoulder is coincident with a feature attributed to $Li_2Mg(NH)_2$ (3180 cm^{-1}) [28]. Also, discussion in

Heyns *et al.*[26] suggests the possibility that the 3207 cm^{-1} peak is consistent with the presence of physisorbed NH_3, especially if the ammonia has some NH_4^+ character due to a hydrogen bonding interaction between the N lone pair and bound hydrogen. The observed position is intermediate between the range of "NH_3 in amino complexes" (3115-3330 cm^{-1}) and NH_4^+ ion (3040 cm^{-1}). We note that we do not observe an accompanying bending mode expected near 1400-1600 cm^{-1}, but this mode would be less intense and may be unobservable against the large background. On the other hand, the ammonia would not be expected to be observed in XRD spectra. Also, as discussed previously, ammonia release occurs in the modified materials, so the presence of the gas in the sample is reasonable.

3.2.3 Conclusions

In this paper, we have compared the effect of compositional modifications on the dehydrogenation/rehydrogenation rates, the temperature of initial hydrogen release and the amount of ammonia released from unmodified and modified 1:1 MgH_2 and $LiNH_2$. The decomposition steps observed in TGA-RGA data support the 3 step reactions listed in literature; however, further studies are needed to determine decomposition pathway. XRD studies indicate that after discharging at 260°C into 1 bar, the resulting mixtures consists of Mg_3N_2, LiMgN. With the addition of $TiCl_3$, VCl_3, $NiCl_2$ or $ScCl_3$, the temperature of initial hydrogen release was reduced; however, Ti and V chlorides also reduced the temperature of ammonia release by promoting a metathesis reaction between $LiNH_2$ and the chlorides. Ni and Sc modified samples showed the highest isothermal absorption capacity followed by unmodified, V and Ti modified samples. After cycling, no discernable kinetic effect remained from the additions. It is concluded that once the metathesis reaction is complete, the added metallic species are no longer active in the sorption cycle. This work has highlighted the requirement of cycling these materials to reach a steady state operating chemistry to evaluate the effectiveness of potential additives as kinetic aids.

4 Reference:

[1] Alapati SV, Johnson JK, Sholl DS. Identification of Destabilized Metal Hydrides for Hydrogen Storage Using First Principles Calculations. The Journal of Physical Chemistry B 2006;110:8769.

[2] Lu J, Fang ZZ, Choi YJ, Sohn HY. Potential of Binary Lithium Magnesium Nitride for Hydrogen Storage Applications. The Journal of Physical Chemistry C 2007;111:12129.

[3] Akbarzadeh AR, V. Ozolins, Wolverton C. First-Principles Determination of Multicomponent Hydride Phase Diagrams: Application to the Li-Mg-N-H System. Advanced Materials 2007;19:3233.

[4] Peles A, Van de Walle CG. Role of charged defects and impurities in kinetics of hydrogen storage materials: A first-principles study. Physical Review B 2007;76:214101.

[5] Majzoub EH, Gross KJ. Titanium-halide catalyst-precursors in sodium aluminum hydrides. Journal of Alloys and Compounds 2003;356-357:363.

[6] Naik M-u-d, Rather S-u, Zacharia R, So CS, Hwang SW, Kim AR, Nahm KS. Comparative study of dehydrogenation of sodium aluminum hydride wet-doped with ScCl3, TiCl3, VCl3, and MnCl2. Journal of Alloys and Compounds 2009;471:L16.
[7] Wronski ZS, Carpenter GJC, Czujko T, Varin RA. A new nanonickel catalyst for hydrogen storage in solid-state magnesium hydrides. International Journal of Hydrogen Energy 2010;In Press, Corrected Proof.
[8] Oelerich W, Klassen T, Bormann R. Metal oxides as catalysts for improved hydrogen sorption in nanocrystalline Mg-based materials. Journal of Alloys and Compounds 2001;315:237.
[9] Malka IE, Czujko T, Bystrzycki J. Catalytic effect of halide additives ball milled with magnesium hydride. International Journal of Hydrogen Energy 2010;35:1706.
[10] Liang G, Huot J, Boily S, Van Neste A, Schulz R. Catalytic effect of transition metals on hydrogen sorption in nanocrystalline ball milled MgH2-Tm (Tm=Ti, V, Mn, Fe and Ni) systems. Journal of Alloys and Compounds 1999;292:247.
[11] Lu J, Choi YJ, Fang ZZ, Sohn HY. Effect of milling intensity on the formation of LiMgN from the dehydrogenation of LiNH2-MgH2 (1:1) mixture. Journal of Power Sources 2010;195:1992.
[12] Wang Q, Chen Y, Niu G, Wu C, Tao M. Nature of Ti Species in the Li-Mg-N-H System for Hydrogen Storage: A Theoretical and Experimental Investigation. Industrial & Engineering Chemistry Research 2009;48:5250.
[13] Song Y, Guo ZX, Yang R. Influence of titanium on the hydrogen storage characteristics of magnesium hydride: a first principles investigation. Materials Science and Engineering A 2004;365:73.
[14] Chen P, Xiong Z, Luo J, Lin J, Tan KL. Interaction of hydrogen with metal nitrides and imides. Nature 2002;420:302.
[15] Luo W, Stewart K. Characterization of NH_3 formation in desorption of Li-Mg-N-H storage system. Journal of Alloys and Compounds 2007;440:357.
[16] Markmaitree T, Osborn W, Shaw LL. Comparisons between MgH_2- and LiH-containing systems for hydrogen storage applications. International Journal of Hydrogen Energy 2008;33:3915.
[17] Liu Y, Zhong K, Gao M, Wang J, Pan H, Wang Q. Hydrogen Storage in a $LiNH_2$-MgH_2 (1:1) System. Chemistry of Materials 2008;20:3521.
[18] Liang C, Liu Y, Luo K, Li B, Gao M, Pan H, Wang Q. Reaction Pathways Determined by Mechanical Milling Process for Dehydrogenation/Hydrogenation of the $LiNH_2/MgH_2$ System. Chemistry – A European Journal 2010;16:693.
[19] Tsuda M, Diño WA, Kasai H, Nakanishi H, Aikawa H. Mg-H dissociation of magnesium hydride MgH2 catalyzed by 3d transition metals. Thin Solid Films 2006;509:157.
[20] Lohstroh W, Fichtner M. Reaction steps in the Li-Mg-N-H hydrogen storage system. Journal of Alloys and Compounds 2007;446-447:332.
[21] DOE Targets for Onboard Hydrogen Storage Systems for Light-Duty Vehicles.
[22] Osborn W, Markmaitree T, Shaw LL. Evaluation of the hydrogen storage behavior of a LiNH2 + MgH2 system with 1:1 ratio. Journal of Power Sources 2007;172:376.

[23] Sandrock G, Gross K, Thomas G. Effect of Ti-catalyst content on the reversible hydrogen storage properties of the sodium alanates. Journal of Alloys and Compounds 2002;339:299.
[24] Santisteban JR, Cuello GJ, Dawidowski J, Fainstein A, Peretti HA, Ivanov A, Bermejo FJ. Vibrational spectrum of magnesium hydride. Physical Review B 2000;62:37.
[25] Kuriyama K, Yamashita Y, Ishikawa T, Kushida K. Raman scattering from the filled tetrahedral semiconductor LiMgN: Identification of the disordered arrangement between Li and Mg. Physical Review B (Condensed Matter and Materials Physics) 2007;75:233204.
[26] Heyns AM, Prinsloo LC, Range K-J, Stassen M. The Vibrational Spectra and Decomposition of α-Calcium Nitride (α-Ca_3N_2) and Magnesium Nitride (Mg_3N_2). Journal of Solid State Chemistry 1998;137:33.
[27] Yamane H, Okabe TH, Ishiyama O, Waseda Y, Shimada M. Ternary nitrides prepared in the Li_3N-Mg_3N_2 system at 900-1000 K. Journal of Alloys and Compounds 2001;319:124.
[28] Hattrick-Simpers JR, Maslar JE, Niemann MU, Chiu C, Srinivasan SS, Stefanakos EK, Bendersky LA. Raman spectroscopic observation of dehydrogenation in ball-milled $LiNH_2$-$LiBH_4$-MgH_2 nanoparticles. International Journal of Hydrogen Energy 2010;In Press, Corrected Proof.